# Anisotropic plastic deformation by viscous flow in ion tracks

T. van Dillen and A. Polman
*FOM-Institute for Atomic and Molecular Physics, Kruislaan 407, NL-1098 SJ Amsterdam, The Netherlands*

P. R. Onck and E. van der Giessen
*Department of Applied Physics, University of Groningen, Nijenborgh 4, NL-9747 AG Groningen, The Netherlands*
(Received 30 June 2004; published 13 January 2005)

A model describing the origin of ion beam-induced anisotropic plastic deformation is derived and discussed. It is based on a viscoelastic thermal spike model for viscous flow in single ion tracks derived by Trinkaus and Ryazanov. Deviatoric (shear) stresses, brought about by the rapid thermal expansion of the thermal spike, relax at ion track temperatures beyond a certain flow temperature. Shear stress relaxation is accompanied by the generation of viscous strains. The model introduces differential equations describing the time evolution of the radial and axial stresses, enabling an exact derivation of the viscous strains for any ion track temperature history $T(t)$. It is shown that the viscous strains effectively freeze in for large track cooling rates, whereas reverse viscous flow reduces the net viscous strains in the ion track for smaller cooling rates. The model is extended to include finite-size effects that occur for ion tracks close to the sample edge, enabling a comparison with experimental results for systems with small size. The "effective flow temperature approach" that was earlier introduced by Trinkaus and Ryazanov by making use of Eshelby's theory of elastic inclusions, follows directly from the viscoelastic model as a limiting case. We show that the viscous strains in single ion tracks are the origin of the macroscopic anisotropic deformation process. The macroscopic deformation rate can be directly found by superposing the effects of single ion impacts. By taking realistic materials parameters, model calculations are performed for experimentally studied cases. Qualitative agreement is observed.

DOI: 10.1103/PhysRevB.71.024103 PACS number(s): 61.43.−j, 61.80.Az, 61.82.Ms, 62.20.Fe

## I. INTRODUCTION

Stress-free amorphous materials subjected to irradiation with ions at energies of ~100 keV and higher exhibit anisotropic plastic flow.[1–7] The anisotropy is related to the direction of the ion beam: materials expand perpendicular to the ion beam and contract parallel to the ion beam while maintaining their volume. The anisotropic deformation is most pronounced at low temperatures (<100 K) and decreases with increasing irradiation temperature.[4,7] The deformation increases with ion fluence at a constant rate, without saturation. It is well established that the deformation is mainly driven by electronic excitations rather than the atomic displacements induced by the ion beam.

Anisotropic deformation has been experimentally investigated in great detail for thin foils of silica and metallic glasses.[3,4] Recently, MeV ion irradiation of micron-sized colloidal silica particles was used to change the colloids' shape from spherical to oblate ellipsoidal.[6–8] The ion irradiation-induced anisotropic deformation technique is now a well-established tool to tailor the shape of nanoscale and microscale structures. It has led to many applications, such as the tailoring of lithographic as well as colloidal nanomasks, tuning the optical bandgap of colloidal photonic crystals, tailoring the plasmon resonance in metallo-dielectric colloids, and controlling the anisotropy of colloidal particles for use in colloidal ordering studies.[9,10]

One of the most successful attempts to describe the deformation process with many of its characteristics is the viscoelastic model derived by Trinkaus *et al.*[11–14] This model, also known as the "*effective flow temperature approach*," describes the viscous relaxation of shear stresses in the cylindrical ion track region. These shear stresses are brought about by the rapid thermal expansion of the ion-induced thermal spike. Complete shear stress relaxation in this region is assumed to take place when the ion track temperature exceeds a certain flow temperature $T^*$. Trinkaus and Ryazanov use Eshelby's theory of ellipsoidal elastic inclusions in elastically isotropic media to calculate the viscous shear strains and assume these to freeze in upon rapid cooling so as to produce the overall anisotropic deformation.[11] Our aim in the current paper is to analyze in detail this stress relaxation process, focusing on the spatial evolution of stress and strain as a function of temperature and time. Along the way, due attention is paid to boundary conditions and approximations.

This paper is organized as follows. After defining the proper type of viscoelastic model and describing the equations and boundary conditions governing the viscous flow in ion tracks (Sec. II), we will first analyze the stresses and strains that develop upon initial thermal loading (Sec. III). Subsequently, in Sec. IV, we will study viscous relaxation by deriving a set of differential equations describing the evolution of the stresses and the viscous strains in ion tracks. This will lead to a general closed-form solution for the viscous strains. Based on these general solutions we will show in Sec. V some examples of time-dependent flow in ion tracks and compare our results with the "*effective flow temperature approach*" approximation. We will also show that ion tracks close to a sample edge exhibit reduced viscous flow compared to ion tracks situated far away from the edges. This

 

result enables a comparison with experiments performed on nanoscale systems with dimensions comparable to that of the ion track. In Sec. VI we will show that the macroscopic deformation (as the result of multiple ion tracks) can be calculated directly from our mesoscopic model, without the necessity of calculating the volume average of the total strain. Finally, in Sec. VII, we will compare the calculated macroscopic deformation rate for silica glass with experimental values.

## II. FORMULATION OF THE MODEL

When an ion penetrates a solid it is slowed down by nuclear and electronic stopping processes.[15] Anisotropic deformation is mainly dependent on the electronic energy loss $F_e$. This excitation/ionization process takes place within $10^{-16}$ s. After local thermalization of the electronic subsystem, energy is transferred from the electronic to the atomic subsystem (electron-phonon coupling)[16–18] at time scales in the range $10^{-14}$–$10^{-12}$ s. The rapid thermal expansion of the track results in large shear stresses in the heated region. For high $F_e$ the heated region around the ion track may become fluid. Due to the reduced viscosity the thermally induced shear stresses relax, resulting in viscous expansion in the plane perpendicular to the ion track. After $\sim 10^{-10}$–$10^{-9}$ s the thermal spike has cooled down to the irradiation (substrate) temperature. For high cooling rates inside the thermal spike, the viscous strain freezes in, leading to anisotropic deformation.[11] In order to describe the viscous flow in ion tracks we now, for the first time, explicitly formulate the assumptions, make the proper choice of viscoelastic model, write down all governing equations, and solve them under appropriate approximations and boundary conditions as listed below.

(1) The electronic stopping $F_e$ is energy dependent and thus changes as a function of depth. However, for high enough ion energies and small enough target thicknesses this depth dependence can be neglected. Indeed, for MeV ion irradiation of colloidal silica particles and the high-energy ion irradiation of thin foils of metallic and silica glasses the variation of $F_e$ with depth is only small. Consequently, also the resulting track temperature $T$ is independent of depth.

(2) Toulemonde *et al.* have calculated the space-time evolution of the temperature distribution in the thermal spike by solving the heat flow equations in the electronic and atomic subsystems that are coupled by the electron-phonon interaction.[13,16–20] It is found that the track temperature $T(r,t)$ ($r$ is the radial coordinate measured from the center of the track) can rise up to several thousand K. In this article we will not take into account these "exact" temperature profiles, but assume that the time-dependent temperature in a cylinder around the ion track ($r \leqslant a$) is uniform (i.e., independent of $r$). The radius of the cylinder, $a$, is determined by the so-called flow temperature $T^*$, the temperature at which the material shows fluid-like behavior at time scales of the thermal spike.[13,14]

The geometry of the ion track in the sample is schematically depicted in Fig. 1. The sample is modeled as a cylindrical disk of height $h$ and radius $b$. An ion penetrates the sample at $r=0$ (along the $z$ axis). As a result of assumptions (1) and (2), a cylindrical region of fixed radius $a$ is uniformly heated.[21] By virtue of the cylindrical geometry of the sketched problem we will use cylindrical coordinates $r$, $\theta$, and $z$ (see Fig. 1).

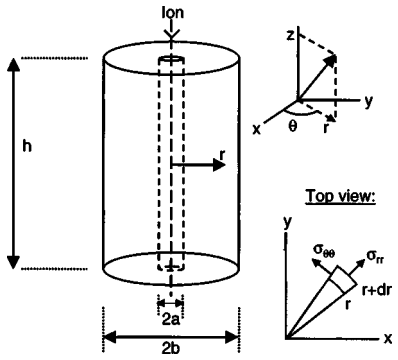


FIG. 1. Geometry of a cylindrical ion track of radius $a$ in a disk (sample) with radius $b$ and height $h$. The cylindrical coordinates $r$, $\theta$, $z$ are indicated in the figure, as well as the stress components $\sigma_{rr}$ and $\sigma_{\theta\theta}$.

(3) The radius $a$ of the thermal spike is typically on the order of several nm.[18,20] The height $h$ of the sample, however, is on the order of several $\mu$m. The aspect ratio of the cylinder, $h/a$, thus is typically $>10^3$. This suggests that the ion track geometry can be described by an infinitely long cylinder of radius $a$ inside a matrix of radius $b$. As a result, at each time during the deformation process, planes remain flat (axial displacement $u_z$ independent of $r$), while the axial strain, $\varepsilon_{zz}=\partial u_z/\partial z$, is independent of $z$. This condition is known as *generalized plane strain*. We will show that for $b \to \infty$ the axial strain vanishes, a condition known as *plane strain*.

(4) The *equations of motion* describing the evolution of a velocity field $v_i$ in a stress field with components $\sigma_{ij}$, are given by (neglecting body forces) $\rho\, dv_i/dt=\partial\sigma_{ij}/\partial x_j$, where we have used Einstein's summation convention and where $\rho$ is the mass density. The inertia forces are only important for describing the emission of elastic waves during the initial stage of the thermal spike and are neglected here. This yields the equations of equilibrium,

$$\frac{\partial \sigma_{ij}}{\partial x_j} = 0. \tag{2.1}$$

(5) To describe anisotropic deformation as a result of the shear stress relaxation by viscous flow in ion tracks, it is important to make the proper choice for the stress-strain relations. The commonly used viscoelastic models are the Kelvin/Voigt model, used in Refs. 22 and 23 and Maxwell's model used by Trinkaus.[14] In the former model a spring (elastic, Hookean element) and a dashpot (viscous, Newtonian element) are coupled in parallel, while they are placed in series in the Maxwell model.

The Kelvin/Voigt model does not allow for complete stress relaxation because of the constraint imposed by the elastic, Hookean element. Here we choose Maxwell's

model in which shear stresses can be relaxed at reduced viscosities leading to concomitant viscous strains. The latter then are the origin of the anisotropic plastic deformation. In Maxwell's model the total strain $\varepsilon_{ij}$ is a superposition of elastic ($\varepsilon_{ij}^{e}$), viscous ($\varepsilon_{ij}^{\nu}$), and thermal ($\varepsilon_{ij}^{th}$) strains, that is

$$\varepsilon_{ij} = \varepsilon_{ij}^{e} + \varepsilon_{ij}^{v} + \varepsilon_{ij}^{th}, \tag{2.2}$$

while it is related to the displacement field $u_i$ in the following way:

$$\varepsilon_{ij} = \frac{1}{2}\left(\frac{\partial u_i}{\partial x_j} + \frac{\partial u_j}{\partial x_i}\right). \tag{2.3}$$

For isotropic elastic media, the elastic strain tensor $\varepsilon_{ij}^{e}$ is coupled to the stress tensor $\sigma_{ij}$ by Hooke's law:

$$\varepsilon_{ij}^{e} = \frac{1}{2\mu}\left(\sigma_{ij} - \frac{\nu}{1+\nu}\sigma_{kk}\delta_{ij}\right), \tag{2.4}$$

where $\mu = E/[2(1+\nu)]$ is the shear modulus, and $E$ and $\nu$ are Young's modulus and Poisson's ratio, respectively. In Eq. (2.4), $\sigma_{kk} = \sigma_{11} + \sigma_{22} + \sigma_{33}$ is the hydrostatic stress (negative pressure), and $\delta_{ij}$ is the Kronecker delta ($\delta_{ij} = 1$ for $i = j$, $\delta_{ij} = 0$ for $i \neq j$). The elastic behavior of the material is therefore described by two independent material parameters $E$ and $\nu$.[24]

The inelastic behavior of the material is described by volume-conserving Newtonian viscous flow through

$$\frac{d\varepsilon_{ij}^{\nu}}{dt} \equiv \dot{\varepsilon}_{ij}^{\nu} = \frac{1}{2\eta}s_{ij}, \tag{2.5}$$

where

$$s_{ij} \equiv \sigma_{ij} - \tfrac{1}{3}\sigma_{kk}\delta_{ij} \tag{2.6}$$

are the components of the stress deviator and $\eta$ is the material's shear viscosity, which is strongly temperature dependent. Note that viscous flow can occur only in a nonhydrostatic (i.e., deviatoric) stress state, $s_{ij} \neq 0$. This is the basis for the phenomenon of shear stress relaxation, although it should be noted that the shear stresses are not relaxed, but the deviatoric stresses are.[25]

Finally, the last term in Eq. (2.2) concerns the thermal strains $\varepsilon_{ij}^{th}$, which are given by

$$\varepsilon_{ij}^{th} = \alpha \Delta T \delta_{ij}, \tag{2.7}$$

where $\alpha$ is the coefficient of linear thermal expansion and $\Delta T = T - T_s$ is the difference between the ion track cylinder's temperature $T$ and the temperature of the substrate $T_s$.

The governing equations (2.1)–(2.5) and (2.7) describe shear stress relaxation through viscous flow inside the ion tracks. When an ion penetrates the sample it rapidly heats up a cylinder of radius $a$. Due to the mismatch in thermal straining (the elastic matrix around the ion track cylinder remains at the substrate temperature $T_s$, so that $\varepsilon_{ij}^{th} = 0$ for $r > a$) and the geometry of the ion track, nonhydrostatic stresses build up. Above a so-defined flow temperature $T^*$, the viscosity $\eta(T)$ inside the ion track cylinder is low enough for the deviatoric stresses to relax, thus introducing viscous strains. Since heating of the ion track cylinder occurs at a time scale to within $\sim 10^{-13}$–$10^{-12}$ s,[13,20] i.e., much smaller than the time scale of viscous flow, the heating can be taken as instantaneous. Therefore, we split the analysis in two parts: a *thermal loading* part (Sec. III), describing the generation of internal stresses due to an instantaneous temperature increase $\Delta T$ (at $t = 0$) in the ion track, and a *viscous relaxation* part (Sec. IV), describing stress relaxation and the associated viscous strain generation determined by the temperature evolution $\Delta T(t)$.

## III. INITIAL STATE: INSTANTANEOUS THERMAL LOADING

The instantaneous thermal loading is a thermoelastic problem that can be solved by starting from the equations of equilibrium (2.1). In case of cylindrical symmetry (no dependence on circumferential angle $\theta$), only a single equilibrium condition is left:[26]

$$\frac{d\sigma_{rr}}{dr} + \frac{\sigma_{rr} - \sigma_{\theta\theta}}{r} = 0. \tag{3.1}$$

The direction of the stresses $\sigma_{rr}$ (radial) and $\sigma_{\theta\theta}$ (hoop) are shown in Fig. 1. The shear stresses $\sigma_{r\theta}$, $\sigma_{rz}$, and $\sigma_{\theta z}$ vanish due to the cylindrical symmetry. In the absence of viscous flow the stress-strain relations given by Eqs. (2.2), (2.4), and (2.7) reduce to

$$\varepsilon_{rr} = \frac{1}{E}[\sigma_{rr} - \nu(\sigma_{\theta\theta} + \sigma_{zz})] + \alpha\Delta T,$$

$$\varepsilon_{\theta\theta} = \frac{1}{E}[\sigma_{\theta\theta} - \nu(\sigma_{rr} + \sigma_{zz})] + \alpha\Delta T, \tag{3.2}$$

$$\varepsilon_{zz} = \frac{1}{E}[\sigma_{zz} - \nu(\sigma_{rr} + \sigma_{\theta\theta})] + \alpha\Delta T.$$

For cylindrical symmetry the radial and hoop total strains, $\varepsilon_{rr}$ and $\varepsilon_{\theta\theta}$, are determined solely by the radial displacement $u_r$ through

$$\varepsilon_{rr} = \frac{du_r}{dr}, \quad \varepsilon_{\theta\theta} = \frac{u_r}{r}. \tag{3.3}$$

In the absence of external forces, the total force in the axial direction, $F_z$, should vanish:

$$F_z = \int_0^b \sigma_{zz}(r) 2\pi r \, dr = 0. \tag{3.4}$$

With Eq. (3.4) and the traction-free boundary condition $\sigma_{rr}(r = b) = 0$, the solutions of Eqs. (3.1)–(3.3) for the normal stress components are found as[26]

$$\sigma_{rr}(r) = \frac{\alpha E}{1-\nu}\left[\frac{1}{b^2}\int_0^b \Delta T(r')r'\,dr' - \frac{1}{r^2}\int_0^r \Delta T(r')r'\,dr'\right],$$

$$\sigma_{\theta\theta}(r) = \frac{\alpha E}{1-\nu}\left[-\Delta T(r) + \frac{1}{b^2}\int_0^b \Delta T(r')r'\,dr' + \frac{1}{r^2}\int_0^r \Delta T(r')r'\,dr'\right], \tag{3.5}$$

$$\sigma_{zz}(r) = \frac{\alpha E}{1-\nu}\left[\frac{2}{b^2}\int_0^b \Delta T(r')r'\,dr' - \Delta T(r)\right].$$

We assume a uniform temperature distribution within the thermal spike region and thus the ion track cylinder of radius $a$ is homogeneously heated to $T_{\max}$ ($\Delta T = T_{\max} - T_s \equiv \Delta T_0$ for $r \leqslant a$) while the surrounding material remains at the temperature $T_s$ ($\Delta T = 0$ for $a < r \leqslant b$). For this specific temperature profile, the stresses inside the ion track cylinder ($r \leqslant a$) from Eqs. (3.5) and the corresponding strains from (3.2) are found to be

$$\sigma_{rr} = \sigma_{\theta\theta} = \tfrac{1}{2}\sigma_{zz} = -\frac{\alpha E \Delta T_0}{2(1-\nu)}(1-\delta^2),$$

$$\varepsilon_{rr} = \varepsilon_{\theta\theta} = \frac{(1+\nu)+\delta^2(1-3\nu)}{2(1-\nu)}\alpha\Delta T_0, \quad \varepsilon_{zz} = \alpha\Delta T_0\delta^2, \tag{3.6}$$

where $\delta \equiv a/b$. The result for $a < r \leqslant b$ is given by[27]

$$\sigma_{rr} = -\frac{\alpha E\Delta T_0}{2(1-\nu)}\left[\left(\frac{a}{r}\right)^2 - \delta^2\right]; \quad \sigma_{\theta\theta} = \frac{\alpha E\Delta T_0}{2(1-\nu)}\left[\left(\frac{a}{r}\right)^2 + \delta^2\right],$$

$$\sigma_{zz} = \frac{\alpha E\Delta T_0}{(1-\nu)}\delta^2,$$

$$\varepsilon_{rr} = -\frac{\alpha\Delta T_0}{2(1-\nu)}\left[(1+\nu)\left(\frac{a}{r}\right)^2 - (1-3\nu)\delta^2\right],$$

$$\varepsilon_{\theta\theta} = \frac{\alpha\Delta T_0}{2(1-\nu)}\left[(1+\nu)\left(\frac{a}{r}\right)^2 + (1-3\nu)\delta^2\right]; \quad \varepsilon_{zz} = \alpha\Delta T_0\delta^2. \tag{3.7}$$

Equations (3.6) and (3.7) fully characterize the stress-strain distribution in the thermal spike and its surrounding material upon instantaneous heating. Figures 2(a) and 2(b) show the stress and strain distributions, respectively, calculated using Eqs. (3.6) and (3.7) for $\delta = 0.25$ and $\nu = 0.2$. The stresses are normalized with $\alpha E\Delta T_0/[2(1-\nu)]$ and the strains with $\alpha\Delta T_0/[2(1-\nu)]$. Figure 2(a) shows that the (compressive) stresses are uniform inside the cylinder of radius $a$. This result also follows from Eshelby's theory of ellipsoidal elastic inclusions as adopted by Trinkaus and Ryazanov.[11] The axial stress ($\sigma_{zz}$) is compressive and is twice as large as the in-plane compressive stresses ($\sigma_{rr}, \sigma_{\theta\theta}$). Since the stress tensor is nonhydrostatic, there are deviatoric stresses $s_{ij}$, which follow from (2.6) and (3.6) to be

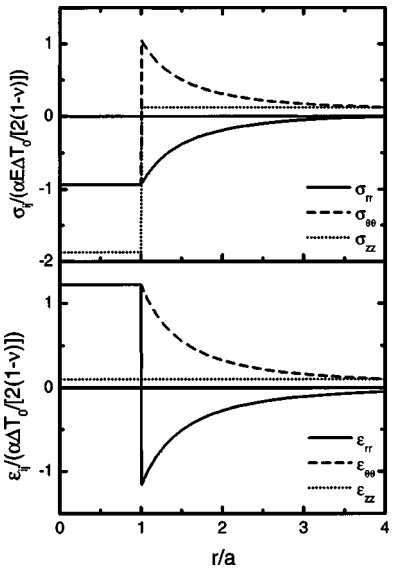


FIG. 2. (a) Distribution of the stresses $\sigma_{rr}$, $\sigma_{\theta\theta}$, and $\sigma_{zz}$, and (b) the strains $\varepsilon_{rr}$, $\varepsilon_{\theta\theta}$, and $\varepsilon_{zz}$ after instantaneous heating and expansion of the ion track cylinder, as a function of $r/a$ [Eqs. (3.6) and (3.7)]. Results are plotted for $\nu = 0.2$ and $b = 4a$ ($\delta = 0.25$).

$$s_{rr} = s_{\theta\theta} = -\tfrac{1}{2}s_{zz} = \frac{\alpha E\Delta T_0}{6(1-\nu)}(1-\delta^2). \tag{3.8}$$

These deviatoric stresses are the driving force for viscous straining according to Eq. (2.5), which will generate negative viscous strains in the axial direction and positive viscous strains in the radial and hoop directions. The details of this relaxation process will be the subject of the next two sections.

In the surrounding material ($a < r \leqslant b$) the stresses and strains decay as $1/r^2$. These solutions are identical to the well-known elastic solution for a thick-walled cylinder under internal pressure.[26] Note that for finite $\delta$ the radial stress vanishes at $r = b$, whereas the hoop stress does not, while $\sigma_{rr} + \sigma_{\theta\theta}$ is uniform in $a < r \leqslant b$.

Figure 2(b) shows that within the heated region, $r \leqslant a$, the strains are uniform. The axial strain $\varepsilon_{zz}$ is indeed constant as was imposed by the condition of "generalized plane strain" (Sec. II). For $\delta \to 0$ it follows from Eqs. (3.6) and (3.7) that $\varepsilon_{zz} = 0$, i.e., "plane strain."

The stress and strain distributions shown in Fig. 2 are the initial conditions (at $t = 0$) for the time-dependent viscous flow in the ion track cylinder, as described next.

## IV. GENERAL TIME-DEPENDENT SOLUTION FOR VISCOUS FLOW IN SINGLE ION TRACKS

After the initial instantaneous heating at $t = 0$, the deviatoric stresses inside the ion track cylinder ($r \leqslant a$) may relax as long as the ion track temperature is above the flow temperature, i.e., $T > T^*$. The governing equations for this stage are different than those leading to the solution discussed in Sec. III, since now the viscous contribution (2.5) to the strain (2.2) needs to be considered.

The equilibrium condition (3.1) is, in general, not sufficient to determine the stress fields, but we can make use of the structure of the initial solution found in Sec. III. Inside the ion track ($r \leqslant a$), $\sigma_{rr}(r;t=0)$ and $\sigma_{\theta\theta}(r;t=0)$ are uniform and equal. Since this holds for the initial state, the equilibrium condition (3.1) remains satisfied identically when

$$\sigma_{rr}(r;t) = \sigma_{\theta\theta}(r;t) = c(t). \tag{4.1}$$

Here $c(t)$ is a function that only depends on time $t$. In Appendix A it is shown that in this case the axial stress $\sigma_{zz}$ is also uniform in this region.

For $a < r \leqslant b$ the initial solution in Eq. (3.7) satisfies $\sigma_{rr}(r;t=0)+\sigma_{\theta\theta}(r;t=0)=\text{const}$. Using this result for each time $t$ and by applying the appropriate boundary conditions,

$$\lim_{r\downarrow a} \sigma_{rr}(r;t) = \sigma_{rr}(a;t),\ \sigma_{rr}(r=b;t) = 0, \tag{4.2}$$

the solution of the equation of equilibrium in $a < r \leqslant b$ is

$$\sigma_{rr}(r;t) = \sigma_{rr}(a;t)\frac{(a/r)^2 - \delta^2}{1-\delta^2},$$

$$\sigma_{\theta\theta}(r;t) = -\sigma_{rr}(a;t)\frac{(a/r)^2 + \delta^2}{1-\delta^2}. \tag{4.3}$$

As a result of Eq. (4.3), $\sigma_{zz}$ is also uniform for $a < r \leqslant b$ (see Appendix A). Since the axial force resultant $F_z$ should vanish in the absence of external forces and by making use of uniformity of the axial stresses in both regions, we find that

$$\sigma_{zz}(a < r \leqslant b;t) = -\sigma_{zz}(a;t)\frac{\delta^2}{1-\delta^2}. \tag{4.4}$$

At this stage we have shown that inside the ion-track cylinder ($r \leqslant a$) all stresses, $\sigma_{rr}=\sigma_{\theta\theta}$ and $\sigma_{zz}$, are uniform (and therefore also all strains) and that in the surrounding elastic material ($a < r \leqslant b$) $\sigma_{zz}$ is uniform, while $\sigma_{rr}$ and $\sigma_{\theta\theta}$ have a radial $1/r^2$ dependence according to Eq. (4.3). Note that through Eqs. (4.3) and (4.4) all stresses in the material follow from the uniform stresses $\sigma_{rr}(a;t)$ and $\sigma_{zz}(a;t)$ inside the ion-track cylinder. To calculate the time evolution of these stresses we use the constitutive equations (2.2)–(2.7) and the following two continuity conditions at $r=a$.

(1) Since the radial displacement $u_r(r;t)$ must be continuous at $r=a$ it follows from Eq. (3.3) that the hoop strain $\varepsilon_{\theta\theta}(r;t)$ should also be continuous at $r=a$:

$$\lim_{r\uparrow a} \varepsilon_{\theta\theta}(r;t) = \lim_{r\downarrow a} \varepsilon_{\theta\theta}(r;t). \tag{4.5}$$

(2) Due to the condition of generalized plane strain [i.e., $\varepsilon_{zz}(r;t)=\varepsilon_{zz}(t)$, independent of $r$]:

$$\lim_{r\uparrow a} \varepsilon_{zz}(r;t) = \lim_{r\downarrow a} \varepsilon_{zz}(r;t). \tag{4.6}$$

For $r \leqslant a$ it follows from Eqs. (2.6) and (4.1) that $s_{rr}=s_{\theta\theta}=-\frac{1}{2}s_{zz}=\frac{1}{3}(\sigma_{rr}-\sigma_{zz})$, so that from Eq. (2.5) the viscous strain rates are uniform, given by

$$\dot{\varepsilon}^{\nu}_{rr}(t) = \dot{\varepsilon}^{\nu}_{\theta\theta}(t) = -\tfrac{1}{2}\dot{\varepsilon}^{\nu}_{zz}(t) = \frac{1}{6\eta(t)}[\sigma_{rr}(t) - \sigma_{zz}(t)], \tag{4.7}$$

with $\eta(t) \equiv \eta(T(t))$. Since $\varepsilon^{\nu}_{ij}(t=0) \equiv 0$ it follows from Eq. (4.7) that $\varepsilon^{\nu}_{rr}(t)=\varepsilon^{\nu}_{\theta\theta}(t)=-\frac{1}{2}\varepsilon^{\nu}_{zz}(t)$ and therefore the total uniform strains $[\varepsilon_{ij}(r;t)=\varepsilon_{ij}(t)]$ in Eqs. (2.2)–(2.7) become

$$\varepsilon_{rr}(t) = \varepsilon_{\theta\theta}(t) = \frac{1}{E}[(1-\nu)\sigma_{rr}(t) - \nu\sigma_{zz}(t)] + \varepsilon^{\nu}_{rr}(t) + \alpha\Delta T(t),$$

$$\varepsilon_{zz}(t) = \frac{1}{E}[\sigma_{zz}(t) - 2\nu\sigma_{rr}(t)] - 2\varepsilon^{\nu}_{rr}(t) + \alpha\Delta T(t). \tag{4.8}$$

For $a < r \leqslant b$, the strain in the elastic surrounding medium is given by Eq. (2.4). Taking the limit for $r \to a$ and by using Eqs. (4.2) and (4.3) we find that

$$\lim_{r\downarrow a} \varepsilon_{rr}(r;t) = \frac{1}{E}\left[\left(1 + \nu\frac{1+\delta^2}{1-\delta^2}\right)\sigma_{rr}(t) + \nu\frac{\delta^2}{1-\delta^2}\sigma_{zz}(t)\right],$$

$$\lim_{r\downarrow a} \varepsilon_{\theta\theta}(r;t) = \frac{1}{E}\left[-\left(\nu + \frac{1+\delta^2}{1-\delta^2}\right)\sigma_{rr}(t) + \nu\frac{\delta^2}{1-\delta^2}\sigma_{zz}(t)\right], \tag{4.9}$$

$$\lim_{r\downarrow a} \varepsilon_{zz}(r;t) = \frac{1}{E}\left[-\frac{\delta^2}{1-\delta^2}\sigma_{zz}(t) + 2\nu\frac{\delta^2}{1-\delta^2}\sigma_{rr}(t)\right],$$

where the stresses $\sigma_{rr}(t)$ and $\sigma_{zz}(t)$ are the uniform stresses $\sigma_{rr}(a;t)$ and $\sigma_{zz}(a;t)$ in the ion-track cylinder. Inserting Eqs. (4.8) and (4.9) into the continuity conditions (4.5) and (4.6) results in two equations for $\sigma_{rr}(t)$, $\sigma_{zz}(t)$ and $\varepsilon^{\nu}_{rr}(t)$. If we then take the time derivative and use Eq. (4.7) to eliminate the viscous strain rates, two differential equations can be obtained for the radial and axial stresses inside the ion track:

$$2\dot{\sigma}_{rr}(t) - \nu\dot{\sigma}_{zz}(t) + \frac{\xi E}{6\eta(t)}[\sigma_{rr}(t) - \sigma_{zz}(t)] + \alpha\xi E\Delta\dot{T}(t) = 0,$$

$$\dot{\sigma}_{zz}(t) - 2\nu\dot{\sigma}_{rr}(t) - \frac{\xi E}{3\eta(t)}[\sigma_{rr}(t) - \sigma_{zz}(t)] + \alpha\xi E\Delta\dot{T}(t) = 0, \tag{4.10}$$

with an initial condition, from Eq. (3.6),

$$\sigma_{rr}(t=0) = \tfrac{1}{2}\sigma_{zz}(t=0) = -\frac{\alpha\xi E\Delta T_0}{2(1-\nu)},$$

with $\xi=1-\delta^2$. An addition of the two equations in a proper way gives a relation between the stress rates. By integrating over time we obtain the following relation between $\sigma_{rr}(t)$ and $\sigma_{zz}(t)$:

$$\sigma_{zz}(t) = -\frac{4-2\nu}{1-2\nu}\sigma_{rr}(t) - \frac{3\alpha\xi E}{1-2\nu}\Delta T(t). \tag{4.11}$$

With the aid of Eq. (4.11), the set of first-order differential equations (4.10) can be reduced to a single second-order differential equation for the radial viscous strain $\varepsilon^{\nu}_{rr}(t)$, through Eq. (4.7):

$$\ddot{\varepsilon}^{\nu}_{rr}(t) + \frac{\dot{\tau}(t)+1}{\tau(t)}\dot{\varepsilon}^{\nu}_{rr}(t) - \frac{1+\nu}{5-4\nu}\frac{\alpha\Delta\dot{T}(t)}{\tau(t)} = 0,$$

$$\varepsilon^{\nu}_{rr}(0) = 0, \quad \dot{\varepsilon}^{\nu}_{rr}(0) = \frac{\alpha\xi E\Delta T_0}{12\eta_0(1-\nu)}, \tag{4.12}$$

where

$$\tau(t) = \frac{12(1-\nu^2)}{5-4\nu}\frac{\eta(t)}{\xi E} \tag{4.13}$$

is the characteristic viscous flow time scale at time $t$, and $\eta_0 = \eta(t=0) = \eta(T(t=0)) = \eta(T_{max})$, is the spike's thermal viscosity at $t=0$. If $T(t)$ and $\eta(T(t))$ are known, the solution of Eq. (4.12) gives a full description of the viscous strains in ion tracks in a virgin sample without external stresses. By integrating Eq. (4.12) twice with respect to time, we find the following closed-form integral solution for $\varepsilon^{\nu}_{rr}(t)$:

$$\varepsilon^{\nu}_{rr}(t) = \frac{1+\nu}{5-4\nu}\alpha\int_0^t \Delta T(t'')\exp\left[-\int_{t''}^{t}\frac{dt'}{\tau(t')}\right]\frac{dt''}{\tau(t'')}. \tag{4.14}$$

This expression allows us to directly calculate the evolution of the viscous strains in both the high-temperature and the (rapid) cooling phase of the ion track cylinder. In the next section we will show how viscous strains are generated at spike temperatures $T > T^*$ and how these strains are frozen in upon subsequent cooling down.

## V. VISCOUS FLOW IN SINGLE ION TRACKS: RESULTS

Calculations of flow in an ion cylinder can be performed by numerically solving the differential equations (4.10) for $\sigma_{rr}$ and $\sigma_{zz}$ and (4.12) for $\varepsilon^{\nu}_{rr}$ [or alternatively, evaluating Eq. (4.14)]. The normalization of these equations allows us to perform general calculations without using specific material-dependent parameters. To this end we have normalized the temperature $T$ with respect to the maximum temperature $T_{max}$ inside the ion track. We used a temperature-dependent shear viscosity $\eta(T)$ of the following empirical form:

$$\eta(T) = \psi 10^{\lambda/T}, \tag{5.1}$$

where $\psi$ and $\lambda$ are material-dependent parameters.[28] In normalizing the temperature with $T_{max}$ in Eqs. (4.10), (4.12), and (4.14), with $\eta$ from Eq. (5.1), we have used the following normalized parameters for our numerical calculations: $T_s/T_{max}=0.025$ and $\lambda/T_{max}=6.8$.[29] Finally, the stresses $\sigma_{ij}$ were normalized with $\alpha E\Delta T_0$, and the time $t$ was normalized with $\tau_0$, the characteristic time for shear stress relaxation in the ion track cylinder at temperature $T_{max}$, given by

$$\tau_0 = \frac{12(1-\nu^2)}{5-4\nu}\frac{\eta_0}{E}. \tag{5.2}$$

In Eq. (5.2), $\eta_0 = \eta(T_{max})$ and Poisson's ratio $\nu$ was chosen to be 0.2, a typical value for, e.g., silica glasses. The value of $\tau_0$ is typically in the order of a few picoseconds.

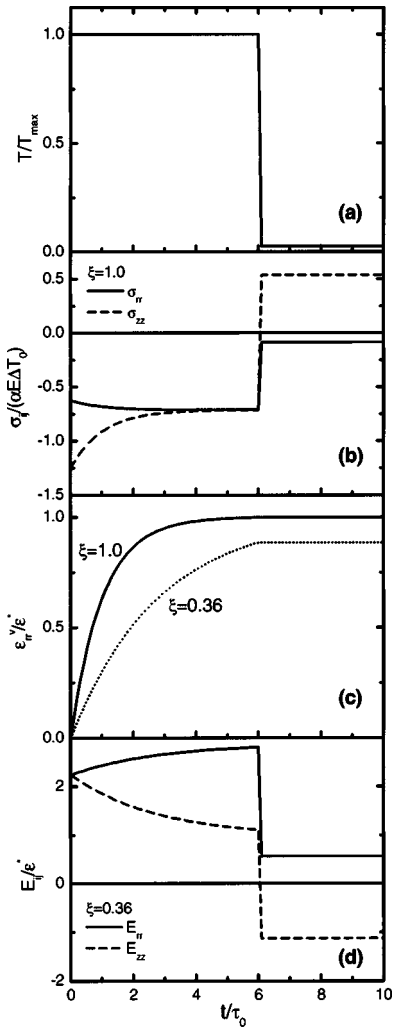


FIG. 3. (a) Time evolution of the ion track temperature $T$, (b) the corresponding stresses $\sigma_{ij}$ [$\sigma_{rr}=\sigma_{\theta\theta}$ (solid line), $\sigma_{zz}$ (dashed line)] for $r \leqslant a$, (c) the associated radial viscous strain $\varepsilon^{\nu}_{rr}$ [for $\xi=1.0$ (solid line), $\xi=0.36$ (dotted line)] for $r \leqslant a$, and (d) the resulting macroscopic deformations $E_{rr}$ (solid line) and $E_{zz}$ (dashed line) for $\xi=0.36$. The time is normalized with $\tau_0$ [Eq. (5.2)]. Results are plotted using $\nu=0.2$, $T_s/T_{max}=0.025$ and $\lambda/T_{max}=6.8$. Stresses are normalized with $\alpha E\Delta T_0$ and the strains in (c) and (d) with $\varepsilon^*$ [Eq. (5.6)]. At the spike lifetime $\tau_s=6\tau_0$ the temperature almost instantaneously drops from $T_{max}$ to the substrate temperature $T_s$.

First we will evaluate a limiting case in which the temperature $T(t)$ inside the ion track remains at a high temperature $T_{max}$ during a time interval $\tau_s$ (spike lifetime) and then (almost) instantaneously drops to the substrate temperature $T_s$. This temperature evolution is shown in Fig. 3(a), where the (normalized) ion track temperature, $T/T_{max}$, is plotted as a function of $t/\tau_0$. In this calculation the spike lifetime $\tau_s$ has been chosen to be $6\tau_0$ to allow for nearly full relaxation of the stresses to their steady-state value. Since the temperature remains constant for $t \leqslant \tau_s$ the differential equations (4.10) and (4.12) can easily be solved analytically since $d\tau(t)/dt=0$ and $d\Delta T(t)/dt=0$. In this case the evolution of the radial stress is given by

$$\sigma_{rr}(t) = \frac{1-2\nu}{2(1-\nu)(5-4\nu)}\alpha\xi E\Delta T_0 \exp\left[-\xi\frac{t}{\tau_0}\right] - \frac{3}{5-4\nu}\alpha\xi E\Delta T_0, \tag{5.3}$$

which reveals that the characteristic relaxation time scale is $\tau_0/\xi = \tau_0/[1-(a/b)^2]$. The axial stress $\sigma_{zz}(t)$ can then be found from Eq. (4.11).

Figure 3(b) shows the result of the numerical calculation of the normalized radial stress $\sigma_{rr}(t)$ (solid curve) and axial stress $\sigma_{zz}(t)$ (dashed curve), as a function of $t/\tau_0$, for the case $\xi=1.0$, i.e., $b \gg a$. The initial values of $\sigma_{rr}$ and $\sigma_{zz}$ are compressive, as given by Eq. (3.6) (normalized values of $-0.625$ and $-1.25$, respectively). During viscous flow, for $0 \leqslant (t/\tau_0) \leqslant (\tau_s/\tau_0) = 6$, the compressive radial stress increases, whereas the compressive axial stress decreases, thereby reducing the deviatoric stresses. As can be seen in Fig. 3(b), this process continues until all stresses are equal ($\sigma_{rr}=\sigma_{\theta\theta}=\sigma_{zz}$) and a negative hydrostatic stress state is achieved. From Eqs. (5.3) and (4.11) it immediately follows that for $\tau_0 \ll t < \tau_s$, this stress is given by

$$\sigma_{rr} = \sigma_{\theta\theta} = \sigma_{zz} = -p = -\frac{3}{5-4\nu}\alpha\xi E\Delta T_0, \tag{5.4}$$

where $p$ is the hydrostatic pressure inside the ion track after stress relaxation. From Eq. (5.4) it follows that the hydrostatic stress state has a pressure of $p/(\alpha E\Delta T_0) = 3\xi/(5\text{-}4\nu) = 0.714$, as can also be seen in Fig. 3(b).

For $0 \leqslant t \leqslant \tau_s$ the viscous strains resulting from the stress relaxation can be found by solving Eq. (4.12) or by directly calculating Eq. (4.14), and are given by

$$\varepsilon^{\nu}_{rr}(t) = \varepsilon^{\nu}_{\theta\theta}(t) = -\tfrac{1}{2}\varepsilon^{\nu}_{zz}(t) = \frac{1+\nu}{5-4\nu}\alpha\Delta T_0\left(1-\exp\left[-\xi\frac{t}{\tau_0}\right]\right). \tag{5.5}$$

Viscous strains thus build up at a characteristic time scale of $\tau_0/\xi$ and saturate at a limiting value of

$$\varepsilon^{\nu}_{rr} = \varepsilon^{\nu}_{\theta\theta} = -\tfrac{1}{2}\varepsilon^{\nu}_{zz} \equiv \varepsilon^{*} = \frac{1+\nu}{5-4\nu}\alpha\Delta T_0. \tag{5.6}$$

This is shown in Fig. 3(c) where the in-plane viscous strain $\varepsilon^{\nu}_{rr}$, normalized with $\varepsilon^*$, is plotted as a function of $t/\tau_0$ for $\xi=1$ (solid curve). Starting at $\varepsilon^{\nu}_{rr}=0$ at $t=0$, the in-plane viscous strain increases and exponentially approaches its saturation value of $\varepsilon^*$, which is reached at the end of the spike lifetime $\tau_s$. Note that the result in Eq. (5.6), which follows from the time-dependent relaxation model as a limiting case, was also found by Trinkaus and Ryazanov in the "effective flow temperature approach."[11]

Next, at $t/\tau_0=6$, the spike instantaneously cools down to the substrate temperature $T_s$ [Fig. 3(a)]. The viscosity $\eta$ thus changes from a small value (liquid) to a relatively large value (solid), abruptly turning off viscous flow. As a result, the viscous strains given by Eq. (5.6) freeze in. This can be seen in Fig. 3(c) where $\varepsilon^{\nu}_{rr}$ does not change upon the instant temperature quenching. As in the case of instantaneous heating (Sec. III) the instantaneous cooling down is a simple elastic problem. The stress field can be derived by using the same continuity conditions at $r=a$ (Sec. IV) and by taking the in-plane frozen-in viscous strain equal to $\varepsilon^*$. This yields the following final stress state:

$$\sigma_{rr} = \sigma_{\theta\theta} = -\frac{1-2\nu}{2(1-\nu)(5-4\nu)}\alpha\xi E\Delta T_0,$$

$$\sigma_{zz} = \frac{2-\nu}{(1-\nu)(5-4\nu)}\alpha\xi E\Delta T_0. \tag{5.7}$$

Figure 3(b) reveals that both stresses abruptly adapt to the instant temperature jump and reach values of $\sigma_{rr}/(\alpha E\Delta T_0) = -0.089$ and $\sigma_{zz}/(\alpha E\Delta T_0) = +0.54$. The compressive radial stress and tensile axial stress are a direct consequence of the frozen-in viscous strains. Since the ion track has viscously expanded perpendicular to the ion beam, the in-plane stress remains compressive ($<0$) whereas the axial stress becomes tensile ($>0$) due to the viscous axial contraction. Said differently, if the ion track would be cut out from its elastic surrounding medium, the only strains within the ion track cylinder would be the viscous strains given by Eq. (5.6). The cylinder would expand freely in the direction perpendicular to the ion track with strain $\varepsilon^*$ and contract in the axial direction with strain $-2\varepsilon^*$ (to conserve volume). Forcing the cylinder back into the surrounding medium would imply that it had to be *compressed* in the in-plane direction (radial and hoop) and to be *pulled* on in the axial direction (tensile stress). Therefore, "an ion track penetrating a thin film acts like a tensioned string tight between the two surfaces of the film."[11]

Figure 3(c) also shows the radial viscous strain as a function of $t/\tau_0$ for $\xi=0.36$ (dotted curve), i.e., a case where the sample's edge at $r=b$ is located close to the ion track cylinder wall ($b=1.25a$). It can be seen that the characteristic time for shear stress relaxation, $\tau_0/\xi$, is now longer. As a consequence, the fully relaxed hydrostatic stress state in the ion track cannot be achieved within the spike lifetime and the viscous strain is frozen in before it has reached its maximum value of $\varepsilon^*$. Ion tracks very close to the edge of a sample therefore should exhibit reduced viscous flow.[30]

The situation described above is a limiting case in which cooling occurs instantaneously. The effect of the cooling rate $dT/dt$ on viscous flow in ion tracks can be studied by the numerical integration of Eq. (4.12). As a first step toward incorporating the effect of a temperature-time profile in the calculations, we study the case for an ion track cylinder that cools down at a constant rate. Figure 4(a) shows an example of the ion track temperature $T$ as a function of $t/\tau_0$, where the temperature again remains constant at $T_{max}$ for $t \leqslant 6\tau_0$, after which the ion track cylinder cools down at a constant rate and reaches $T_s$ at $t=60\tau_0$. All parameters used for this calculation are equal to those used in Fig. 3, i.e., $T_s/T_{max}=0.025$, $\lambda/T_{max}=6.8$, $\nu=0.2$, and $\xi=1.0$. The solid line in Fig. 4(b) shows the calculated normalized in-plane viscous strain $\varepsilon^{\nu}_{rr}/\varepsilon^*$ as a function of $t/\tau_0$. For comparison, the dashed line in Fig. 4(b) shows $\varepsilon^{\nu}_{rr}/\varepsilon^*$ for infinitely large cooling rates and is identical to the solid line in Fig. 3(c). For

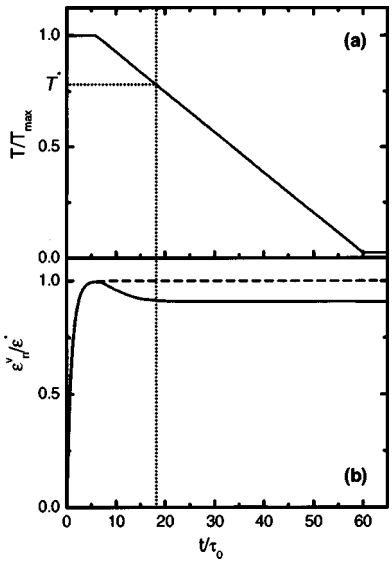


FIG. 4. (a) Time evolution of the ion track temperature $T$, and (b) the corresponding radial viscous strain $\varepsilon_{rr}^{\nu}$ (solid line) for $r \leqslant a$. The time is normalized with $\tau_0$, the characteristic time for shear stress relaxation in ion track cylinders at temperature $T_{max}$ situated far away from the sample's edge [Eq. (5.2)]. Results are plotted using: $\nu=0.2$, $T_s/T_{max}=0.025$, $\lambda/T_{max}=6.8$, and $\xi=1$. The viscous strain is normalized with $\varepsilon^*$ [Eq. (5.6)]. The dashed curve in (b) represents the radial viscous strain upon instantaneous freezing in [the solid line in Fig. 3(c)]. Between $6\tau_0$ and $60\tau_0$ the temperature decreases from $T_{max}$ to $T_s$ at a constant rate $dT/dt$. The dotted lines indicate the time and the effective flow temperature $T^*$ at which the viscous strains freeze in.

$6\tau_0 \leqslant t \leqslant 60\tau_0$ the temperature in the spike decreases, which again introduces deviatoric stresses in the ion track. Since $\sigma_{rr}-\sigma_{zz}$ becomes negative, the in-plane viscous strain rate, $d\varepsilon_{rr}^{\nu}/dt$, is now negative according to Eq. (4.7). Therefore, the material will exhibit viscous flow in the opposite direction (with respect to the flow for $t \leqslant 6\tau_0$) in order to relax these deviatoric stresses, shown by the initial decrease in the solid curve of Fig. 4(b). As the temperature continues to decrease, the viscosity increases until it becomes too large for reverse viscous flow to continue on the time scale of the thermal spike. Hence, the in-plane viscous strain freezes in at a value smaller than $\varepsilon^*$, depending on the cooling rate $dT/dt$ and the temperature dependence of the viscosity, $\eta(T)$. In this particular example, the effective frozen-in viscous strain is $0.91\varepsilon^*$ (solid line), 9% lower than the value for infinitely large cooling rates (dashed line). From Fig. 4 we can estimate the effective flow temperature $T^*$, below which no stress relaxation occurs at the time scale of the thermal spike; it amounts to $\sim 0.8T_{max}$ in this example (dotted lines).

To estimate the value of $T^*$ for a commonly irradiated material like silica glass, a material that exhibits large anisotropic plastic deformation under ion irradiation,[4,7] the characteristic time scale $\tau$ for viscous flow in ion tracks, Eq. (4.13), can be set equal to the characteristic thermal spike lifetime $\tau_s$.[14] For $SiO_2$ containing 0.12 wt.% water, the viscosity (in Pa s) below about 1800 K is specified as[31]

$$\log_{10}\eta = -7.7 + \frac{2.67\times 10^4}{T}, \tag{5.8}$$

with the temperature $T$ in K. If we extrapolate Eq. (5.8) for temperatures higher than 1800 K and use typical elastic parameters for silica, $\nu=0.2$ and $\mu=34$ GPa ($E=81.6$ GPa),[32] the estimated value of $T^*$ is between 3250 and 3750 K when using typical thermal spike lifetimes between $10^{-11}$ s and $10^{-10}$ s.[13] This implies that for irradiation conditions in which the thermal spike temperature does not reach $\sim$3500 K, no anisotropic deformation is expected.

In the preceding sections, we have derived an exact model to solve the anisotropic strain in a *single* ion track cylinder, assuming a homogeneous temperature distribution in the spike for a spike duration $\tau_s$, and a subsequent temperature quenching profile. Experimental data on anisotropic deformation are only available on systems that have had *multiple* ion impacts. For example, the well-characterized deformation of spherical colloidal particles with diameters of $\sim 1$ $\mu$m is the overall effect of some $10^6$–$10^7$ ions impacting on a single colloid.[6] In the next section we will describe how such a macroscopic effect can be derived from the mesoscopic model introduced above.

## VI. FROM MESOSCOPIC MODEL TO MACROSCOPIC DEFORMATION

To show that the local viscous flow in single ion tracks is the origin of the macroscopic deformation process, we have to determine the change in the macroscopic sample dimensions due to successive ion impacts.

Our sample is a disk of radius $b$ and height $h$, as sketched in Fig. 1. During a *single* ion-induced thermal spike having an internal radial viscous strain of $\varepsilon_{rr}^{\nu}(t)$, the radius of the sample changes with $\Delta b(t)$ and its height with $\Delta h(t)$. From Eq. (3.3) it follows that $\Delta b(t)=u_r(b;t)=b\varepsilon_{\theta\theta}(b;t)$, so that the macroscopic radial strain $E_{rr}(t)$ can be written as

$$E_{rr}(t) = \frac{\Delta b(t)}{b} = \varepsilon_{\theta\theta}(b;t). \tag{6.1}$$

The macroscopic axial strain $E_{zz}(t)$ in the direction of the ion beam during a single ion impact can be found in a similar manner and reads as

$$E_{zz}(t) \equiv \frac{\Delta h(t)}{h} = \varepsilon_{zz}(t). \tag{6.2}$$

We can therefore directly calculate the macroscopic strains $E_{rr}$ and $E_{zz}$ resulting from a single ion impact using the mesoscopic model described in the previous sections. For the calculated example shown in Fig. 3(c) with $b=1.25a$ ($\delta=0.8$ or $\xi=0.36$, dotted line) the result is shown in Fig. 3(d), where $E_{rr}$ (solid line) and $E_{zz}$ (dashed line) are plotted as a function of $t/\tau_0$. This plot is obtained by numerically solving $\sigma_{rr}(t)$ and $\sigma_{zz}(t)$ from Eq. (4.10), substituting the solutions into Eqs. (4.3) and (4.4), and finally by using $\varepsilon_{\theta\theta}$ and $\varepsilon_{zz}$ from Eq. (2.4) at $r=b$.

Figure 3(d) shows that just after the abrupt temperature increase at $t=0$ the macroscopic strains (for a single ion impact) are equal and given by

$$E_{rr}(t=0) = E_{zz}(t=0) \equiv \alpha \Delta T_0 \delta^2, \tag{6.3}$$

which follows directly from Eq. (3.7). Next, for $0 \leqslant t \leqslant \tau_s$, $E_{rr}$ increases during deviatoric stress relaxation resulting from the in-plane viscous expansion $[\varepsilon^{\nu}_{rr}(t) > 0]$, whereas $E_{zz}$ decreases due to the axial viscous contraction $[\varepsilon^{\nu}_{zz}(t) = -2\varepsilon^{\nu}_{rr}(t) < 0]$. Finally, at $t = \tau_s$, the viscous strains freeze in during instantaneous temperature quenching, resulting in a net macroscopic expansion perpendicular to the ion beam, $E_{rr} > 0$, and a net contraction parallel to the ion beam, $E_{zz} = -2E_{rr} < 0$.

In case the ion track cylinder has a frozen-in radial viscous strain of $\varepsilon^*$,[33] the frozen-in macroscopic strains in Eqs. (6.1) and (6.2) after a single ion impact can be directly calculated using Eqs. (5.7), (4.3), (4.4), and (2.4), resulting in

$$E_{rr} = -\tfrac{1}{2} E_{zz} \equiv \varepsilon^* * \delta^2. \tag{6.4}$$

Equation (6.4) clearly shows that the macroscopic deformation is volume conserving.

After $N$ *independent* ion impacts[34] distributed *randomly*,[35] over the sample surface, the total macroscopic deformation is simply a superposition of the individual "total" strains. Recognizing that $N = \pi b^2 \phi$, where $\phi$ is the ion fluence, we can rewrite the macroscopic deformation as

$$E_{rr} = \pi a^2 \varepsilon^* * \phi = -\tfrac{1}{2} E_{zz}. \tag{6.5}$$

Equation (6.5) immediately demonstrates that in the present model the viscous flow in single ion tracks is the origin of the macroscopic deformation process.

We point out that our derivation of the macroscopic deformations directly from the single-ion results is notably different from the averaging procedure adopted by Trinkaus, albeit yielding the same result.[14]

The rate of macroscopic deformation, $A$, defined as the differential length change perpendicular to the ion beam per unit ion fluence, is given by

$$A \equiv \frac{\partial E_{rr}}{\partial \phi} = \varepsilon^* * \pi a^2, \tag{6.6}$$

according to Eq. (6.5). The value of $A$ can be computed once the radius of the ion track is known. For an estimate, let us assume that the initial temperature distribution has the form of a delta function along a linear ion track. Then the track temperature at a distance $r$ from the ion track at time $t$ can be found by solving the classical heat conduction law and is given by[36]

$$T(r;t) = \frac{\Omega}{t} \exp\left[ -\Lambda \frac{r^2}{t} \right] + T_s, \tag{6.7}$$

with $\Omega = F_e'/(4\pi\kappa)$ and $\Lambda = \rho C/(4\kappa)$. Here $F_e'$ is the part of the electronic stopping $F_e$ that is converted to heat in the cylindrical thermal spike region, $\rho$ is the mass density of the material, $\kappa$ is the thermal conductivity, $C$ is the specific heat capacity, and $T_s$ is the substrate temperature. It is shown in Appendix B that for this Gaussian temperature distribution the following relation can be found between the spike's cross section $\pi a^2$ and the flow temperature $T^*$:

$$\pi a^2 = \frac{\pi \Omega}{e \Lambda \Delta T^*} = \frac{F_e'}{e \rho C \Delta T^*}, \tag{6.8}$$

where $e = \exp(1)$ and $\Delta T^* = T^* - T_s$. When the (time-dependent) temperature distribution inside the track is uniform, the uniform in-plane viscous strain $\varepsilon^{\nu}_{rr}$ at the end of a thermal spike is equal to $\varepsilon^*$ [see Eq. (5.6)] for large track cooling rates. In the case of large cooling rates but a nonuniform temperature distribution, we may replace Eq. (5.6) by an appropriate average,

$$\varepsilon^{\nu}_{rr} = \frac{1+\nu}{5-4\nu} \alpha \langle \Delta T \rangle, \tag{6.9}$$

where $\langle \Delta T \rangle$ is the space- and time-averaged temperature increase in the thermal spike. In Appendix B it is shown that, for a Gaussian temperature distribution, $\langle \Delta T \rangle$ is given by[37]

$$\langle \Delta T \rangle = 1.26 (T^* - T_s). \tag{6.10}$$

Replacing $\varepsilon^*$ in Eq. (6.6) by $\varepsilon^{\nu}_{rr}$ from Eq. (6.9) and by substituting Eqs. (6.8) and (6.10), the steady-state deformation rate $A$ now reads as

$$A \equiv \frac{1.26}{e} \frac{1+\nu}{5-4\nu} \frac{\alpha F_e'}{\rho C}. \tag{6.11}$$

## VII. DISCUSSION: COMPARISON WITH EXPERIMENT

### A. *A* at very high energy and low substrate temperature

Klaumünzer *et al.* studied the expansion of silica foils under 360 MeV Xe ion irradiation at 100 K and determined $A = (8.0 \pm 0.5) \times 10^{-16}$ cm$^2$/ion.[38] Taking $F_e'$ equal to the corresponding stopping of $F_e = 15.1$ keV/nm and using typical material parameters of $\nu = 0.2$, $\alpha = 0.6 \times 10^{-6}$ K$^{-1}$, $\rho = 2.2 \times 10^3$ kg m$^{-3}$ and $C = 10^3$ J kg$^{-1}$ K$^{-1}$, Eq. (6.11) yields $A = 8.7 \times 10^{-16}$ cm$^2$/ion, which is in close agreement with the experimental result. Using Eq. (6.8) with $\Delta T^* \approx 3500$ K for silica, the estimated radius of the ion track cylinder is $\sim$6 nm, which is close to the radius found by Toulemonde *et al.* in their thermal spike calculation for silica (at $F_e = 15.1$ keV/nm).[18]

### B. Energy dependence of *A*

As was shown for colloidal silica particles, significant anisotropic deformation is observed at energies as low as 300 keV,[7] and a linear increase of A with $F_e$ is experimentally observed. This is in direct agreement with Eq. (6.11). The increase of $A$ with $F_e$ is brought about by the increasing cylindrical track radius $a$ [see Eqs. (6.6) and (6.8)].

### C. Threshold $F_e$ for anisotropic deformation

It has been experimentally observed for some silica as well as metallic glasses that no deformation occurs below a threshold electronic stopping, typically around 2 keV/nm.[4,38] This is in contrast to what we found for colloidal silica, where no threshold is observed.[7] One explana-

tion for this difference may be the relatively low value of the flow temperature $T^*$ for colloidal silica compared to that of other amorphous materials. Indeed, the bulk melting temperature of colloidal silica is several hundred K below that of fused silica.

### D. Substrate temperature dependence of *A*

As was shown previously, $A$ decreases with increasing irradiation substrate temperature by a factor 4.5 between 85 and 380 K for colloidal silica particles,[7] similar to what was found by Klaumünzer *et al.* for silica and metallic glasses.[1,4] A decrease with increasing temperature is in agreement with the viscoelastic model: the deviatoric stress resulting from the thermal spike [see Eqs. (2.6) and (5.7)] can be partly relaxed at elevated substrate temperatures. Additional calculations must be done to quantitatively study this effect.

Summarizing the comparison between experiment and theory above, we conclude that the viscoelastic model provides an excellent qualitative and often quantitative representation of experimental results.

## VIII. CONCLUSIONS

We have performed a detailed investigation of a viscoelastic thermal spike model describing viscous flow in ion tracks as the origin of anisotropic deformation. First, the track geometry and the imposed condition of "generalized plane strain" were discussed. After assigning Maxwell's model as the physical relevant model, the governing equations describing the flow were discussed in detail. By dividing the analysis in a thermal loading and viscous relaxation part, we solved the equations yielding the time evolution of the stresses and (viscous) strains for a specific track temperature history $T(t)$. A closed-form expression for the radial viscous strains in ion tracks has been found.

We have shown that for large track cooling rates the viscous strains freeze in effectively, while for smaller cooling rates reverse flow reduces the net viscous strains in the ion track. The model also demonstrates that ion tracks close to the edge exhibit reduced viscous flow with respect to tracks located far away from the edge.

As a limiting case, for sufficiently large thermal spike lifetimes and instantaneous temperature quenching, the "effective flow temperature approach" as introduced by Trinkaus and Ryazanov follows directly from the viscoelastic model. For $SiO_2$ the effective flow temperature $T^*$, at which the viscous strains effectively freeze in, is about 3500 K.

Next, we have shown that the frozen-in viscous strains of individual ion impacts are the origin of the macroscopic anisotropic deformation process. In particular, the macroscopic deformation rate can be calculated directly from the mesoscopic model by considering multiple, independent ion tracks randomly penetrating the sample.

Based on a Gaussian temperature profile the macroscopic deformation rate has been calculated. For vitreous silica irradiated with 360 MeV Xe ions at low irradiation temperatures the experimentally observed deformation rate by Klaumünzer *et al.* agrees well with the calculated value from the viscoelastic model. Finally, the experimental dependence of the deformation rate on electronic stopping $F_e$ and irradiation substrate temperature $T_s$ is discussed and shows qualitative agreement with the viscoelastic model.

## ACKNOWLEDGMENTS

This work is part of the research program of the Foundation for Fundamental Research on Matter (FOM) and was financially supported by the Dutch Organization for Scientific Research (NWO). We thank Dr. S. Klaumünzer (Hahn-Meitner-Institut, Berlin) and Dr. H. Trinkaus (Research Center, Jülich) for many fruitful discussions.

## APPENDIX A: UNIFORMITY OF THE AXIAL STRESS

To show that the axial stress $\sigma_{zz}$ is uniform for $r \leqslant a$, we write Hooke's law, Eq. (2.4) for isotropic elastic media, in the form

$$\sigma_{ij} = 2\mu\varepsilon^e_{ij} + \lambda\varepsilon^e_{kk}\delta_{ij}, \tag{A1}$$

where $\lambda = k - (2/3)\mu$ is Lamé's constant and $k = E/[3(1-2\nu)]$ the bulk modulus of elasticity. Using Eqs. (A1), (2.2), and (2.7) we then obtain

$$\begin{aligned}
\sigma_{rr} &= 2\mu(\varepsilon_{rr} - \varepsilon^\nu_{rr}) + \lambda\varepsilon_{kk} - 3k\alpha\Delta T,\\
\sigma_{\theta\theta} &= 2\mu(\varepsilon_{\theta\theta} - \varepsilon^\nu_{\theta\theta}) + \lambda\varepsilon_{kk} - 3k\alpha\Delta T,\\
\sigma_{zz} &= 2\mu(\varepsilon_{zz} - \varepsilon^\nu_{zz}) + \lambda\varepsilon_{kk} - 3k\alpha\Delta T,
\end{aligned} \tag{A2}$$

making use of the fact that viscous strains are volume preserving, i.e., $\varepsilon^\nu_{kk} = 0$. Since $\sigma_{rr} = \sigma_{\theta\theta}$ [Eq. (4.1)] and $\varepsilon^\nu_{rr} = \varepsilon^\nu_{\theta\theta}$ [Eq. (4.7)], it follows from Eq. (A2) that $\varepsilon_{rr} = \varepsilon_{\theta\theta}$. From Eq. (3.3) it immediately follows that both $\varepsilon_{rr}$ and $\varepsilon_{\theta\theta}$ are uniform as well. By taking the time derivative of axial stress in Eq. (A2) and substituting Eq. (4.7), we can now write, for $r \leqslant a$,

$$\dot{\sigma}_{zz} + \frac{2\mu}{3\eta}\sigma_{zz} = 2\mu\dot{\varepsilon}_{zz} + \frac{2\mu}{3\eta}\sigma_{rr} + \lambda(2\dot{\varepsilon}_{rr} + \dot{\varepsilon}_{zz}) - 3k\alpha\Delta\dot{T}. \tag{A3}$$

All terms on the right-hand side of Eq. (A3) are clearly uniform. Since $\sigma_{zz}(t=0)$ is uniform [Eq. (3.6)], it follows from Eq. (A3) that $\sigma_{zz}$ is uniform at each time $t$.

For the elastic surrounding medium, $a < r \leqslant b$, it follows from Eq. (A2) with $\Delta T = 0$,

$$\begin{aligned}
\sigma_{rr} &= 2\mu\varepsilon_{rr} + \lambda\varepsilon_{kk},\\
\sigma_{\theta\theta} &= 2\mu\varepsilon_{\theta\theta} + \lambda\varepsilon_{kk},\\
\sigma_{zz} &= 2\mu\varepsilon_{zz} + \lambda\varepsilon_{kk},
\end{aligned} \tag{A4}$$

that

$$\sigma_{rr} + \sigma_{\theta\theta} = 2(\mu + \lambda)(\varepsilon_{rr} + \varepsilon_{\theta\theta}) + 2\lambda\varepsilon_{zz}. \tag{A5}$$

According to Eq. (4.3), $\sigma_{rr} + \sigma_{\theta\theta}$ is uniform and from Eq. (A5) it then follows that $\varepsilon_{rr} + \varepsilon_{\theta\theta}$ is uniform and therefore $\varepsilon_{kk}$ as well. Thus, $\sigma_{zz}$ is also uniform over $a < r \leqslant b$.

### APPENDIX B: THERMAL SPIKE'S CROSS-SECTION AND AVERAGE TEMPERATURE

For the Gaussian temperature profile given by Eq. (6.8) the maximum temperature at radial distance $r$ is

$$T_{\max}(r) = \frac{\Omega}{e\Lambda r^2} + T_s, \tag{B1}$$

occurring at $t=\Lambda r^2$. The radius $r=a$ is defined as the radius of the cylinder where the maximum temperature $T_{\max}$ just reaches the flow temperature $T^*$ at time $t=t^*$. Hence,

$$\pi a^2 = \frac{\pi\Omega}{e\Lambda\Delta T^*}, \tag{B2}$$

with $\Delta T^* = T^* - T_s$.

Since viscous strains are generated at temperatures above the flow temperature $T^*$, the appropriate average track temperature increase $\langle\Delta T\rangle$ can be found by averaging the temperature difference $\Delta T(r;t)$ over space and time where $T \geqslant T^*$, starting at $t=t^*$. We therefore consider the region $r \leqslant R(t) \leqslant a$ with its boundary, specified by $T(R(t);t)=T^*$, moving towards the center. At time $t \geqslant t^* = \Lambda a^2 = \Omega/(e\Delta T^*)$ the radius $R(t)$ of the region for which $T \geqslant T^*$ is given by

$$R(t) = \sqrt{\frac{t}{\Lambda}\ln\left[\frac{\Omega}{\Delta T^* t}\right]} = a\sqrt{\frac{t}{t^*}\left(1+\ln\left[\frac{t^*}{t}\right]\right)}. \tag{B3}$$

Since $0 \leqslant R(t) \leqslant a$, the time interval for which the track temperatures exceed $T^*$ therefore equals $t^* \leqslant t \leqslant et^*$. First, we determine the spatial average at a fixed time $t$ over the region $r \leqslant R(t)$:

$$\langle\Delta T\rangle(t) \equiv \frac{1}{\pi R^2(t)}\int_0^{R(t)} \Delta T(r;t)\,2\pi r\,dr = \frac{e - t/t^*}{(t/t^*)(1-\ln[t/t^*])}\Delta T^*. \tag{B4}$$

Next, the average track temperature increase $\langle\Delta T\rangle$ can be found by averaging this mean value $\langle\Delta T\rangle(t)$ over the relevant time interval $t^* \leqslant t \leqslant et^*$, resulting in

$$\langle\Delta T\rangle \equiv \frac{1}{t^*(e-1)}\int_{t^*}^{et^*}\langle\Delta T\rangle(t)\,dt = \frac{\Delta T^*}{e-1}\int_1^e \frac{e-x}{x(1-\ln[x])}\,dx = 1.26\Delta T^*. \tag{B5}$$


[1] S. Klaumünzer and G. Schumacher, Phys. Rev. Lett. **51**, 1987 (1983).
[2] S. Klaumünzer, Radiat. Eff. Defects Solids **110**, 79 (1989).
[3] M.-D. Hou, S. Klaumünzer, and G. Schumacher, Phys. Rev. B **41**, 1144 (1990).
[4] A. Benyagoub, S. Löffler, M. Rammensee, S. Klaumünzer, and G. Saemann-Ischenko, Nucl. Instrum. Methods Phys. Res. B **65**, 228 (1992).
[5] A. Audouard, J. Dural, M. Toulemonde, A. Lovas, G. Szenes, and L. Thomé, Phys. Rev. B **54**, 15 690 (1996).
[6] E. Snoeks, A. van Blaaderen, T. van Dillen, C. M. van Kats, M. L. Brongersma, and A. Polman, Adv. Mater. (Weinheim, Ger.) **12**, 1511 (2000).
[7] T. van Dillen, A. Polman, C. M. van Kats, and A. van Blaaderen, Appl. Phys. Lett. **83**, 4315 (2003).
[8] T. van Dillen, A. Polman, W. Fukarek, and A. van Blaaderen, Appl. Phys. Lett. **78**, 910 (2001).
[9] E. Snoeks, A. van Blaaderen, T. van Dillen, C. M. van Kats, K. Velikov, M. L. Brongersma, and A. Polman, Nucl. Instrum. Methods Phys. Res. B **178**, 62 (2001).
[10] K. P. Velikov, T. van Dillen, A. Polman, and A. van Blaaderen, Appl. Phys. Lett. **81**, 838 (2002).
[11] H. Trinkaus and A. I. Ryazanov, Phys. Rev. Lett. **74**, 5072 (1995).
[12] H. Trinkaus, Nucl. Instrum. Methods Phys. Res. B **107**, 155 (1996).
[13] A. Benyagoub, S. Klaumünzer, and M. Toulemonde, Nucl. Instrum. Methods Phys. Res. B **146**, 449 (1998).
[14] H. Trinkaus, Nucl. Instrum. Methods Phys. Res. B **146**, 204 (1998).
[15] J. F. Ziegler, J. P. Biersack, and U. Littmark, *The Stopping and Range of Ions in Solids* (Pergamon, New York, 1985).
[16] M. Toulemonde, C. Dufour, and E. Paumier, Phys. Rev. B **46**, 14 362 (1992).
[17] M. Toulemonde, Ch. Dufour, A. Meftah, and E. Paumier, Nucl. Instrum. Methods Phys. Res. B **166–167**, 903 (2000).
[18] M. Toulemonde, C. Dufour, E. Paumier, and F. Pawlak, Mater. Res. Soc. Symp. Proc. **504**, 99 (1999).
[19] M. Toulemonde, Ch. Dufour, Z. Wang, and E. Paumier, Nucl. Instrum. Methods Phys. Res. B **112**, 26 (1996).
[20] M. Toulemonde, J. M. Costantini, Ch. Dufour, A. Meftah, E. Paumier, and F. Studer, Nucl. Instrum. Methods Phys. Res. B **116**, 37 (1996).
[21] Since shear stress relaxation by viscous flow in ion tracks is the origin of the deformation process and since the viscosity is generally a strongly activated function of temperature [e.g., Eq. (5.8) for silica], shear stresses relax for each $r \leqslant a$ in case the ion track temperature $T(r;t)$ is higher than the effective flow temperature $T^*$ for a spike lifetime $\tau_s$ longer than the characteristic time scale for viscous flow $\tau_0$ (see Sec. V). It is therefore reasonable to assume a constant temperature distribution in the ion track to estimate the local (viscous) deformations. The actual local track temperature $T(r;t)$ should in this case be integrated over space and time to yield the average, "uniform" temperature in the ion track determining the local viscous deformation (see Sec. VI and Appendix B).
[22] A. I. Ryazanov, A. E. Volkov, and S. Klaumünzer, Phys. Rev. B **51**, 12 107 (1995).
[23] V. A. Borodin, A. E. Volkov, and D. N. Korolev, Nucl. Instrum. Methods Phys. Res. B **209**, 122 (2003).

[24] Generally, the elastic moduli depend on temperature. For example, Polian *et al.* have studied the elastic properties of liquid $SiO_2$ up to 2300 K by Brillouin spectroscopy measurements [A. Polian, D. Vo-Thanh, and P. Richet, Europhys. Lett. **57**, 375 (2002)]. It was found that the shear modulus $\mu$ of liquid $SiO_2$ is 34 GPa at 2300 K, which is only 10% larger than the value of 31 GPa found for solid $SiO_2$ at 293 K. Consequently, we assume the elastic moduli to be temperature independent, so that the same moduli can be used inside and outside the ion track.

[25] In the cylindrical coordinate system used here (see Fig. 1), all shear stresses ($\sigma_{r\theta}, \sigma_{rz}, \sigma_{\theta z}$) vanish due to symmetry (Sec. III), while the deviatoric stresses do not. However, shear stresses do exist, albeit on coordinate axes that are rotated with respect to the cylindrical coordinate axes used here.

[26] A. C. Ugural and S. K. Fenster, *Advanced Strength and Applied Elasticity*, 3rd ed. (Prentice–Hall PTR, Englewood Cliffs, NJ, 1995).

[27] To calculate the strains for $a < r \leqslant b$, Eq. (3.2) can be used with $\Delta T = 0$.

[28] See, e.g., Eq. (5.8) for vitreous silica.

[29] The quantity $\psi$ cancels out in normalizing Eqs. (4.10), (4.12), and (4.14).

[30] Ion tracks close to the sample's edge of course do not exhibit the axial symmetry as in our calculations: the edge is not symmetrically located around the ion track. In addition, $\tau_s$ might be larger close to the sample's edge. However, the frozen-in (in-plane) viscous strain, given by $\varepsilon^*(1-\exp[-\xi\tau_s/\tau_0])$, still gives a lower limit estimate for the reduced viscous strains in ion tracks close to the edge.

[31] N. P. Bansal and R. H. Doremus, *Handbook of Glass Properties* (Academic Press, New York, 1986).

[32] A. Polian, D. Vo-Thanh, and P. Richet, Europhys. Lett. **57**, 375 (2002).

[33] This is not the case for the example plotted in Fig. 3(d), as can be seen from the associated in-plane viscous strain plotted in Fig. 3(c) (dotted line).

[34] Independent ion tracks are ion tracks that do not overlap and do not "feel" each other's stress field.

[35] This suggests that on average each ion can be viewed to have its impact at the center of the sample having a distance $b$ to the edge (provided that $b$ is not too close to $a$).

[36] G. H. Vineyard, Radiat. Eff. **29**, 245 (1976).

[37] The value of the average depends on how the average is taken. Our result is slightly different from the one found by Trinkaus and Ryazanov (Ref. 11).

[38] S. Klaumünzer, Nucl. Tracks Radiat. Meas. **19**, 91 (1991).